



This work was carried out in whole or in part within the framework of the NOMATEN Center of Excellence, supported from the European Union Horizon 2020 research and innovation programme (Grant Agreement No. 857470) and from the European Regional Development Fund via the Foundation for Polish Science International Research Agenda PLUS programme (Grant No. MAB PLUS/2018/8).

This is a copy of the publication which appeared in: Corrosion Science, Volume 220, 1 August 2023, 111271, published on: 17 May 2023.

DOI: [10.1016/j.corsci.2023.111271](https://doi.org/10.1016/j.corsci.2023.111271)



Corrosion resistance of β -phase titanium alloys under simulated inflammatory conditions: Exploring the relevance of biocompatible alloying elements

A. Sotniczuk^{a,b,*}, J.L. Gilbert^c, Y. Liu^c, M. Matczuk^d, W. Chromiński^{a,b}, D. Kalita^b, M. Pisarek^e, H. Garbacz^{a,**}

^a Faculty of Materials Science and Engineering, Warsaw University of Technology, Woloska 141, 02-507 Warsaw, Poland

^b NOMATEN Centre of Excellence, National Centre for Nuclear Research, A. Soltana 7, 05-400 Otwock-Swierk, Poland

^c The Clemson University-Medical University of South Carolina Bioengineering Program, 68 President Street, BE 325, Charleston, SC 29425, United States

^d Chair of Analytical Chemistry, Faculty of Chemistry, Warsaw University of Technology, Noakowskiego 3, 00-664 Warsaw, Poland

^e Laboratory of Surface Analysis, Institute of Physical Chemistry, Polish Academy of Sciences, Kasprzaka 44/52, 01-224 Warsaw, Poland

ARTICLE INFO

Keywords:

- A. Titanium
- B. EIS
- B. TEM
- B. XPS
- B. AFM
- C. Interfaces

ABSTRACT

In this study we compared the corrosion behavior of single β -phase alloys: (i) Ti-29Nb-13Ta-4.6Zr and (ii) Ti-45Nb, that contain similar amount of β -phase stabilizers. Corrosion resistance was analyzed in the PBS+H₂O₂ solution, which simulates the conditions as can be found during post-operative inflammation. Results of electrochemical impedance spectroscopy, and ion-release measurements revealed that Ti-29Nb-13Ta-4.6Zr alloy demonstrated significantly higher corrosion resistance compared to Ti-45Nb. Post-immersion microscopic analysis demonstrated that a thinner layer of oxidation products was formed on Ti-29Nb-13Ta-4.6Zr alloy surface. Overall results allowed to exclude the beneficial role of Nb in tailoring corrosion resistance of Ti-29Nb-13Ta-4.6Zr under simulated inflammatory conditions.

1. Introduction

In our aging society, demand is continually increasing for long-lasting implantable devices such as orthopedic or dental implants. Currently, a relatively new group of metastable Ti β -phase alloys is being studied extensively with regard to their application for permanent implants [1–7]. Their attractiveness results from their ultra-low stiffness, which reduces the risk of the stress-shielding effect [2,4,8]. This undesirable phenomenon is associated with diminished stresses being transferred from the biomaterial to the adjacent bone, which can lead to bone resorption around the implant, and/or in the worst case to the implant becoming loose [9]. One of the first multicomponent metastable Ti β -phase alloys was Ti-29Nb-13Ta-4.6Zr (TNTZ), proposed by Niinomi et. al in 1998 [10]. The stiffness of TNTZ alloy (in the solution-treated state) is much lower ($E_{\text{TNTZ}}=60\text{--}62$ GPa) [11,12] than that of the biomaterials currently used for permanent implants ($E_{\text{CoCr}}=200\text{--}220$ GPa, $E_{\text{Ti,Ti6Al4V}}=100\text{--}120$ GPa) [5,8,13]. Moreover, the β -phase in TNTZ alloy is relatively stable, which provides an opportunity to perform

additional mechanical treatments without the risk of undesirable phase transformations that could consequently increase its stiffness [7,14,15]. Additional benefits of TNTZ alloy are its advantageous biological and corrosion performance [7,16]. All of the alloying elements in TNTZ alloy are biocompatible, non-genotoxic, and non-carcinogenic [2]. According to the results of in vitro tests (using hOBs or MG63 cells), TNTZ alloy (in the solution-treated state) demonstrated a cellular response similar to that of typical Ti-based biomaterials [15,17]. Moreover, TNTZ alloy also exhibited high corrosion resistance in the standard solutions used for testing biomaterials, such as minimum essential media (MEM) or simulated body fluid (SBF) [18,19].

Our previous research showed that the oxide layer that forms in air on the TNTZ alloy surface shows unique stability under inflammatory conditions (PBS+H₂O₂) [7,20]. It was found that TNTZ alloy demonstrated better short-term corrosion resistance in PBS+H₂O₂ compared with standard commercially pure Ti (CP-Ti) having different microstructures and crystallographic textures [7,21]. Acute inflammation, which lasts about one week, is an inevitable part of immunological

* Corresponding author at: Faculty of Materials Science and Engineering, Warsaw University of Technology, Woloska 141, 02-507 Warsaw, Poland.

** Corresponding author.

E-mail addresses: agata.sotniczuk@pw.edu.pl (A. Sotniczuk), halina.garbacz@pw.edu.pl (H. Garbacz).

response [22]. A desirable effect of this process is to eliminate pathogens introduced and to trigger the healing of tissue damaged during the invasive implantation procedure [20]. During inflammatory reaction, immunological cells, that are recruited to inflamed site (e.g. neutrophils or macrophages [23]), produce reactive oxygen species (ROS) such as H_2O_2 . It has to be mentioned that inflammatory products (such as H_2O_2) can accelerate the corrosion of metallic biomaterials, including commonly used Ti-based biomaterials such as CP-Ti and its two-phase Ti-6Al-4V alloy [22,24–32]. Analysis of retrieved orthopedic implants, fabricated from Ti-6Al-4V, revealed inflammatory-induced selective dissolution of the β -phase [33]. This was confirmed by further top-view microscopic observations of the Ti-6Al-4V surfaces corroded in the H_2O_2 -rich biological solutions using scanning electron microscopy (SEM) and atomic force microscopy (AFM) [34]. Further research was devoted to analyze H_2O_2 -induced degradation of Ti-6Al-4V by microscopic observations on its cross-section, using the combination of focused ion beam and scanning electron microscopy (FIB-SEM) [26]. Recent study has shown that privileged degradation of β -phase can be observed under cathodic polarization of Ti-6Al-4V [35]. Implant's materials could undergo to the cathodic domain during tribocorrosion events, that typically occur during the lifespan of orthopedic replacements [30]. Thereby, nowadays a huge attention is paid to understand the mechanisms of Ti-6Al-4V degradation induced by tribocorrosion which is known also as mechanically assisted corrosion [36–38]. Metal ions released into the peri-implant environment can stimulate further, undesirable chronic inflammatory processes. It was found that the wear debris, released to the peri-implant environment, could induce the new phenotype of macrophages, which accelerates the degradation of metallic implants [39]. Thereby, interaction between the implant's surface and biological response can be described as a two-way positive feedback mechanism (corrosion of the metal or wear debris generated during tribocorrosion induce inflammation, and inflammation induces further corrosion of the implant) [22]. Reducing the metal dissolution induced by H_2O_2 is essential to avoid a cascade of unwanted chronic inflammatory reactions [40].

One hypothesis that explains the enhanced short-term corrosion properties of TNTZ in the presence of inflammatory products (compared with standard CP-Ti) is the lower number of anion vacancies in the oxide layer formed on its surface [7]. The alloying elements that stabilize the β phase in Ti-based alloys (e.g. Nb and Ta), have higher valences than Ti. The presence of Nb_2O_5 or Ta_2O_5 can compensate for the presence of anion vacancies in the oxygen-deficient Ti oxide layer associated with a certain amount of TiO and Ti_2O_3 [41]. This permits the assumption that a relatively high oxide layer stability under simulated inflammation should also be achievable in the case of the widely studied binary β -phase alloys from the Ti-Nb system [42–46]. One of the most frequently studied alloys from the binary Ti-Nb system is Ti-45Nb [1,42,44,47]. Like TNTZ, Ti-45Nb offers lower stiffness than standard Ti-based biomaterials ($E_{Ti-45Nb} \approx c.a. 70$ GPa – solution-treated state [1]). The main focus of this study, then, was to compare the time-dependent corrosion resistance under simulated inflammatory conditions ($PBS+H_2O_2$) of two, widely investigated biomedical β -phase Ti alloys: binary Ti-45Nb and quaternary Ti-29Nb-13Ta-4.6Zr. This enabled us to verify whether the origin of the relatively high stability of TNTZ alloy in $PBS+H_2O_2$ is associated with a reduction in Ti dissolution due to the presence of alloying elements with higher valences than Ti.

2. Materials and methods

2.1. Materials and microstructural characterization

In order to obtain single β -phase alloys of homogenous chemical composition and similar microstructures, the as-received quaternary and binary alloys were subjected to homogenization (heat treatment) and fast cooling (solution treatment) in water. The homogenization parameters were as follows: (i) TNTZ: 950 °C/30 min, (ii) Ti-Nb:

1000 °C/120 min. Before the heat treatment, both samples were enclosed in glass capsules filled with argon in order to avoid surface oxidation. The microstructure of the samples was characterized using a Hitachi SU-70 Scanning Electron Microscope (SEM) in the Electron Backscattered Diffraction (EBSD) mode. The samples subjected to the EBSD measurements were ground up to #1200 and ion-milled using a Hitachi IM 4000.

2.2. Solutions and corrosion tests

Corrosion tests (both electrochemical and immersion) were performed in pure PBS enriched with H_2O_2 ($PBS+0.1\% H_2O_2$). Firstly, a pure PBS solution was made by dissolving PBS tablets (Sigma Aldrich, $pH=7.2-7.6$) in distilled water. Then, in order to simulate inflammatory conditions, a few droplets of H_2O_2 (30 wt% in H_2O , Sigma Aldrich) were added to the PBS solution in order to obtain $PBS+0.1\% H_2O_2$. Considering the unstable nature of H_2O_2 , all of the solutions were prepared directly before the corrosion tests.

Electrochemical tests were conducted using an Autolab PGSTAT 302 N potentiostat/galvanostat connected to a three-electrode system in which a saturated Ag/AgCl electrode acted as the reference electrode (RE), a graphite rod was the counter electrode (CE), and TNTZ or Ti-Nb alloy acted as the working electrode (WE). The surface area of WE exposed to the solution was the same for all samples (0.1 cm^2) and was limited by the home-made Teflon element. The electrochemical response of the tested alloys was evaluated based on: (i) monitoring of the open circuit potential (OCP) values, (ii) electrochemical impedance spectroscopy (EIS) tests. The EIS tests were performed after 2 h, 24 h, 48 h and 336 h of immersion. All of the EIS tests were carried out at OCP with an amplitude ± 10 mV and a frequency range of 10,000–0.005 Hz. Analysis of the EIS results was performed with NOVA software (version 2.1.4) which enabled to designate (i) the numerical values of electrochemical parameters, (ii) estimated errors related to the fitting of particular electrical elements and (iii) chi-square values for selected electrical circuits.

Additionally, the samples were subjected to the immersion tests in $PBS+H_2O_2$ for the same time-points as in the case of the EIS tests. Immersion tests were performed in sterile, disposable Falcon tubes (1 mL of $PBS+H_2O_2$ per 1 cm^2 of the sample). After completing the immersion tests, the remaining solutions were collected and used in ICP-MS tests. In case of both EIS and ICP-MS, the solution was not changed during the whole immersion period. The solutions collected from Falcon tubes were digested using nitric acid (HNO_3 , 69 %, Fluka, Trace metal basis) for 30 min, diluted in water with yttrium as an internal standard ($10\text{ }\mu\text{g/L}$ final concentration, Sigma-Aldrich) and filtered using $0.45\text{ }\mu\text{m}$ syringe filters prior to analysis. The total concentration of metals (Ti, Nb, Ta, Zr) in the samples was determined using an inductively coupled plasma tandem mass spectrometer working as an element-specific detector. An Agilent 8900 ICP Triple Quadrupole Mass Spectrometer (Tokyo, Japan) was equipped with a 2.5 mm quartz torch and Pt-cones in the interface. The position of the torch and the nebulizer gas flow were adjusted daily, with emphasis paid to increasing the signal-to-noise ratio using a $1\text{ }\mu\text{g/L}$ solution of Co, Y, and Tl in 2 % (v/v) HNO_3 and 2 % (v/v) HNO_3 , respectively. The RF power was 1550 W, nebulizer gas flow – 1.10 L/min , reaction gases flows (the mixture of hydrogen and oxygen) – 8,0 and 0,1 mL/min [48], respectively. The total concentrations of the selected metals were calculated as a result of monitoring the Q1 and Q2 mass/charge ratio changes: $48Ti \rightarrow 64Ti$, $90Zr \rightarrow 106Zr$, $93Nb \rightarrow 109Nb$, $181Ta \rightarrow 197Ta$ registered in the shift-mass mode after the production in the plasma and collision-reaction cell of singly-positively charged ions, recalculating the isotopes' natural abundances, and normalizing ($89Y \rightarrow 105Y$) after daily external calibration against 10-point calibration lines ($0-500\text{ }\mu\text{g/L}$, with minimum $R^2 > 0.9990$).

The samples for all the corrosion tests (electrochemical and ion-release measurements) were ground up to #4000 and polished with a silica suspension (OP-S, Struers) using an automatic polishing machine.

The ICP-MS samples were polished on both sides. After preparation, the surfaces of the samples were ultrasonically cleaned, first with isopropanol and then with distilled water. The cleaned samples were dried with compressed air and put into a desiccator for 2 h before their immersion in the PBS+H₂O₂ solution. For the ICP-MS tests, the samples were enclosed in sterile disposable centrifuge tubes filled with particular solutions (1 mL/1 cm² of the alloy surface). Both the electrochemical and immersion tests were conducted in an incubator at a constant temperature of 37 °C.

2.3. Surface analysis

The surface analysis included characterizing the topography, chemical composition and thickness of the oxide layers formed on the TNTZ and Ti-Nb alloy surfaces. The samples' topography was analyzed using AFM analysis (with a Bruker Dimension ICON). AFM investigations were performed in the contact mode using a ScanAsyst-Fluid probe. The chemical composition was characterized based on the results of an XPS analysis (with a Thermo Electron Microlab 350). The XPS measurements were performed using a non-monochromatic X-ray exciting source with an energy of 1486.6 eV at a power of 300 W. The HR-XPS spectra were solved using Avantage software (Thermo Fisher Scientific) using the Gauss-Lorentz function with a constant G/L ratio = 0.35 (+/- 0.05). The background was corrected using a Smart model. A quantitative analysis of the content of particular states was performed considering Scofield data. Analysis conditions were as follows: (i) Ti2p (Ti oxides): energy difference between spins 3/2 and 1/2–5.54 ± 0.2 eV, peak area ratio 2:1, (ii) Ti⁰ (metallic Ti): energy difference 6.17 ± 0.2 eV (2:1), (iii) Nb3d (Nb oxides and metallic Nb): energy difference between 5/2 and 3/2–2.72 ± 0.2 eV, peak area ratio 3:2, (iv) Ta4f (Ta oxide and metallic Ta): energy difference between 7/2 and 5/2–1.91 ± 0.2 eV, area ratio 4:3, and (v) Zr3d (Zr oxide and metallic Zr): energy difference between 5/2 and 3/2–2.43 ± 0.2 eV, peak area ratio 3:2. The binding energy for all of the detected chemical elements was corrected considering the carbon peak C1s = 285.0 eV. The final results were normalized to 100 % for metallic elements to show the share of individual oxides in the oxide layers.

The chemical composition profiles, which made it possible to assess the thickness of the oxide layers, were evaluated based on the AES analysis (with a Thermo Electron Microlab 350). The oxide atomic monolayers were progressively removed using Ar⁺ ions with the following parameters: beam energy: 2 keV, beam current c.a. 1 µA, etched area: 3 × 3 mm. The ion etching rate, evaluated based on the SiO₂/Si standard, was about 0.09 nm/s. Additionally, the thickness and phase structure of the oxide layers after alloys' exposure to the simulated inflammatory environment was analyzed based on TEM and HR-TEM observations respectively. Electron transparent samples for the TEM studies were prepared by a Focused Ion Beam (FIB) lift-out technique using a Helios 5 UX DualBeam (Thermo Fisher Scientific) microscope. During thinning, the beam acceleration voltage was gradually decreased to 2 kV in order to minimize the impact of Ga ions on the microstructure of the materials. Transmission electron microscopy observations were carried out with Thermo Fischer Scientific Spectra 200 operated at 200 kV.

2.4. Statistical Analysis

In order to verify whether the differences within the designated values of the oxide layer resistances and the amount of the metallic ions released are statistically important, a one-way analysis of variance (ANOVA) together with post hoc Tukey tests were performed. It was assumed that the difference at $p < 0.01$ can be considered to be highly significant [1]. For all of the EIS and ICP-MS measurements at least three independent samples from each group were tested.

3. Results

3.1. Microstructural features

The EBSD studies revealed that Ti-Nb and TNTZ alloys contained equiaxed β-phase grains (Fig. 1), with the following average size and grain size distribution: (i) Ti-Nb: Avg (d₂) = 79 µm, SD (d₂) = 49 µm, (ii) TNTZ: Avg (d₂) = 93 µm, SD (d₂) = 53 µm. Obtaining similar grain sizes of the β phase in the Ti-Nb and TNTZ alloys was possible by subjecting the materials to solution treatment at 1000 °C and 950 °C for the binary and quaternary alloys, respectively. It is well known that the microstructure of the substrate, mainly the phase structure and grain size, can affect the properties of protective air-formed passive layers, and thereby the corrosion resistance of Ti and its alloys [49,50]. Therefore, in order to compare the corrosion resistance of the Ti-Nb and TNTZ alloys only with regard to their chemical composition, it was necessary to eliminate the possible impact of differences in their microstructural features that could affect their electrochemical behavior.

3.2. Corrosion resistance under simulated inflammatory conditions (PBS+H₂O₂)

A quantitative comparison of the corrosion resistance of Ti-Nb and TNTZ was performed based on both electrochemical impedance spectroscopy (EIS) and ion-release measurements (ICP-MS). The EIS studies were conducted under steady state conditions (OCP potential). For both alloys, virtually no changes in the OCP values were observed within the first 48 h of immersion in the PBS+H₂O₂ (Table 1). Prolonged exposure to simulated inflammatory conditions did result in a slight increase in the OCP value (for c.a. 0.2 V for Ti-Nb and c.a. 0.15 V for TNTZ). This slight growth in the OCP value could be related to the suppression of anodic reaction (oxidation of Ti and alloying elements) and thickening of the corrosion products layer during prolonged immersion of the alloys in the PBS+H₂O₂.

The EIS studies were performed as a function of exposure time, precisely after 2 h, 24 h, 48 h and 336 h of immersion of the material in a solution that simulates inflammatory conditions (Fig. 2). Performing EIS tests after different exposure times made it possible to gain knowledge about the evolution of the properties of the oxide layer during prolonged exposure to PBS+H₂O₂. Bode Plots illustrating the results of the EIS tests are presented in Fig. 2. Symmetry of the phase angle part of the Bode plots across the frequency indicated that simple, single-time constant electrical circuit, (Randles-Constant Phase Element, Randles-CPE) should correctly describe electrochemical behavior of tested alloys [51]. The validity of Randles-CPE circuit was confirmed also by finding the lowest fitting errors designated for particular elements, amongst the electrical circuits that were previously used for analysis of the corrosion behavior of biomedical alloys under simulated inflammation: R(RQ)(RQ) [52], R(Q[RW]) [53], and R(Q[W(RC)]) [27]. The physical meaning of the Randles-CPE circuit elements are as follows: (i) R_s corresponds to the PBS+H₂O₂ resistance, (ii) R_{ox} describes oxide layer resistance, and (iii) CPE is correlated to the capacitance of the real, non-ideal oxide layer that could contain some impurities, a certain level of roughness and surface defects. CPE is represented by two parameters (Q and n) which, together with R_{ox} and R_s could be exploited to calculate the effective capacitance (C_{eff}) according to the equation described by Brug et.al. [54,55].

$$C_{eff} = \left[Q \left(\frac{1}{R_s} + \frac{1}{R_{ox}} \right)^{n-1} \right]^{1/n} \quad (1)$$

This type of equation has been exploited, e.g., to describe the semi-conductive properties of the titanium alloys tested in the simulated physiological solutions [3,56]. The values of C_{eff} calculated are in a range of 10⁻⁶ F × cm⁻² (Table 2). The statistical analysis performed did not reveal any significant differences between the C_{eff} values calculated

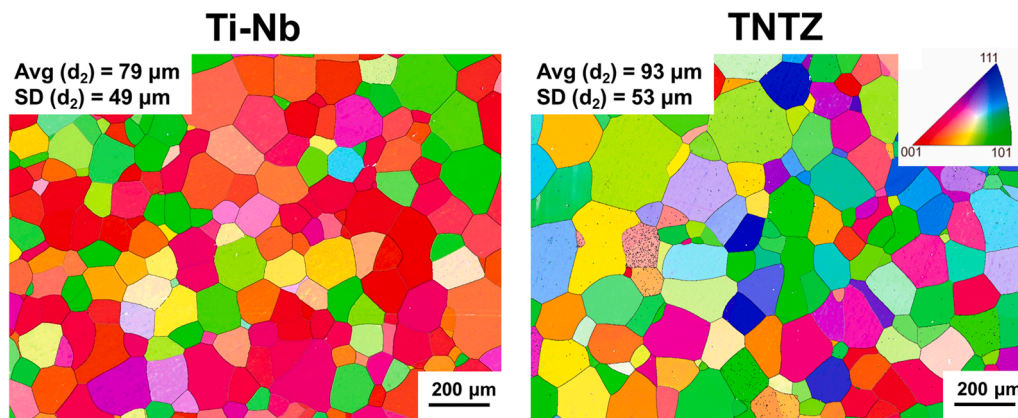


Fig. 1. Microstructure of tested binary and quaternary alloys: EBSD results.

Table 1
OCP variations during Ti-Nb and TNTZ immersion in PBS+H₂O₂.

	2 h	OCP [V] 24 h	48 h	336 h
Ti-Nb	-0.22 ± 0.02	-0.25 ± 0.02	-0.25 ± 0.01	-0.03 ± 0.02
TNTZ	-0.21 ± 0.02	-0.17 ± 0.02	-0.17 ± 0.04	-0.02 ± 0.01

for the Ti-Nb and TNTZ alloys, or between the values designated for particular alloys after different immersion times in PBS+H₂O₂ (Table 2). Almost unvaried C_{eff} values during the immersion of both Ti-Nb and TNTZ alloys indicate that the compact oxide layer that was formed on their surfaces did not change its thickness during the whole immersion time in the simulated inflammatory conditions. On the other hand, prolonged, two-week exposure in PBS+H₂O₂ resulted in an increase in the R_{ox} values calculated for Ti-Nb and TNTZ (from 10⁴ to 10⁵ Ohm × cm²) (Table 2, Fig. 3). This indicates an enhancement of the oxide layer properties after the initial H₂O₂-induced corrosion attack. Similar

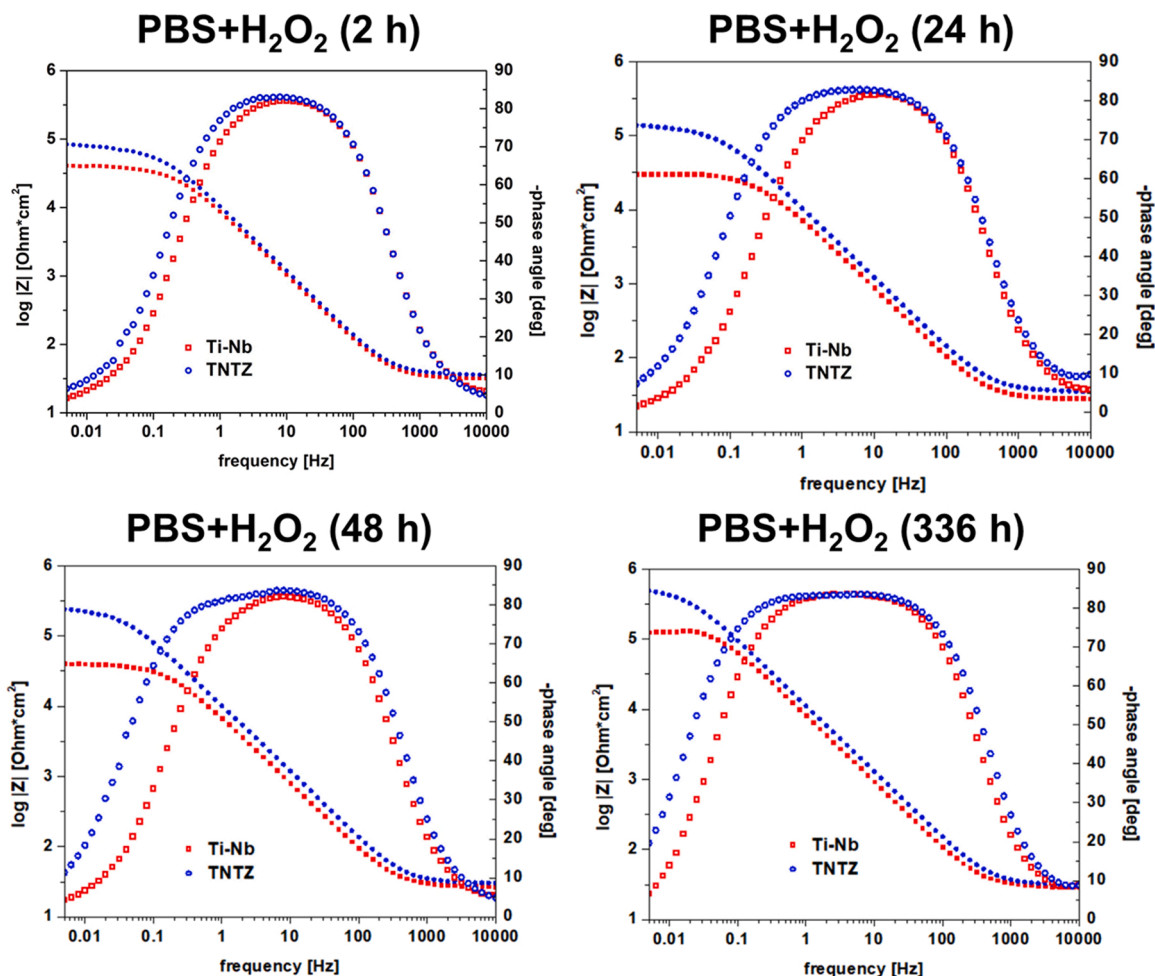
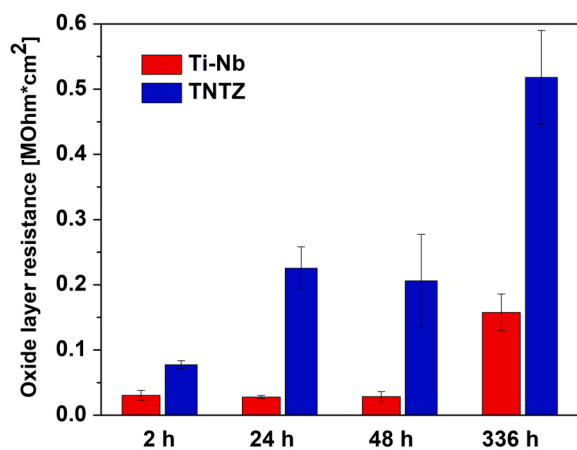


Fig. 2. Bode plots illustrating EIS results performed in PBS+H₂O₂ after different immersion times.

Table 2

Electrochemical parameters calculated from the EIS results (maximum fitting errors of particular EIS parameters are provided in brackets).

	Time [h]	Q [$\times 10^{-5} \Omega^{-1} \text{cm}^{-2} \text{s}^n$]	n	C _{eff} [$\times 10^{-6} \text{F cm}^{-2}$]	R _{ox} [MOhm $\times\text{cm}^2$]	χ^2_{max}
Ti-Nb	2	2.22 \pm 0.39 (0.71 %)	0.93 (0.17 %)	5.74 \pm 2.58	0.03 \pm 0.008 (0.84 %)	0.02
	24	3.14 \pm 0.93 (0.78 %)	0.93 (0.17 %)	7.63 \pm 1.11	0.03 \pm 0.002 (0.69 %)	0.02
	48	3.71 \pm 0.78 (0.77 %)	0.92 (0.17 %)	7.72 \pm 1.25	0.03 \pm 0.007 (0.77 %)	0.03
	336	2.18 \pm 0.05 (0.46 %)	0.94 (0.11 %)	6.86 \pm 0.32	0.16 \pm 0.028 (1.07 %)	0.02
TNTZ	2	1.95 \pm 0.45 (0.67 %)	0.94 (0.15 %)	5.75 \pm 0.53	0.08 \pm 0.006 (0.92 %)	0.02
	24	1.72 \pm 0.15 (0.61 %)	0.94 (0.17 %)	4.78 \pm 0.73	0.23 \pm 0.032 (1.53 %)	0.03
	48	1.86 \pm 0.26 (0.49 %)	0.94 (0.12 %)	6.12 \pm 0.73	0.21 \pm 0.071 (0.87 %)	0.02
	336	2.00 \pm 0.29 (0.49 %)	0.94 (0.12 %)	6.05 \pm 0.46	0.52 \pm 0.072 (1.54 %)	0.03

**Fig. 3.** Oxide layer resistance calculated from the results of the EIS tests performed in PBS+H₂O₂.

results were previously observed for CP-Ti [21,27] and Ti-6Al-4V [52]. An analysis of the time-dependent variation of the R_{ox} value revealed differences in behavior between the Ti-Nb and TNTZ alloys (Fig. 3). For the binary alloy, the R_{ox} values calculated from the EIS tests performed after 2 h of immersion were close to 0.03 MOhm $\times\text{cm}^2$ and did not change significantly during the first 48 h of immersion in PBS+H₂O₂. The growth in the R_{ox} value (by one order of magnitude) took place between 48 h and 336 h of exposure (Fig. 3). In contrast, in the case of the TNTZ alloy, a rapid increase in R_{ox} (from c.a. 0.08–0.23 MOhm $\times\text{cm}^2$) was observed within the first 24 h, and the R_{ox} value then stabilized over the next 24 h of immersion in the solution

(Fig. 3). Prolonged immersion of TNTZ in PBS+H₂O₂ (up to 336 h) resulted in further growth in the R_{ox} value. Apart from the differential characteristic of the time-dependent evolution of R_{ox}, differences were also found between the numerical values of the resistance of the oxide layer calculated for the alloys (Fig. 3). The EIS data revealed that, for all of the analyzed immersion times, the R_{ox} value was greater for the quaternary TNTZ alloy ($p < 0.01$). Therefore, it can be concluded that the corrosion resistance of the TNTZ alloy is significantly greater than that of the Ti-Nb alloy. In order to confirm this finding, the levels of corrosion resistance of TNTZ and Ti-Nb were then compared by means of spectrometric measurements that made it possible to calculate the total amount of metallic ions released during the samples' exposure to PBS+H₂O₂.

The calculated average values of particular types of released ions (in the mmol/cm² [57]) are presented in Table 3 and Fig. 4. The ICP-MS tests revealed that, in both tested alloys, the majority of metallic ions were released during the first 48 h of immersion (Table 3, Fig. 4). The less pronounced increase in the amount of metallic ions released during the further immersion period could be related to a progressive decomposition of the H₂O₂ and thereby a reduction in the oxidation power of the solution; this was previously reported, e.g., for CP-Ti [27]. It can be noticed that, for all immersion times, the total amount of ions released from the Ti-Nb alloy was noticeably higher than from the TNTZ alloy ($p < 0.01$). Moreover, the concentration of Ti ions was more significant in the case of the binary alloy ($p < 0.01$), despite its having a metallic Ti content similar to that of the quaternary alloy. Comparing the amount of particular chemical elements released to the PBS+H₂O₂, with chemical composition of the alloys, allows to verify if any preferential dissolution takes place. For both alloys, the proportion of released ions was close to the bulk composition ratio in the metallic substrates (Ti-30Nb at%, and Ti-20Nb-4.6Ta-3.2Zr at%). This trend was observed in case of the whole

Table 3The average concentration values and standard deviation [mmol/cm²] of metallic ions released into the PBS+H₂O₂ solution after different immersion times (n = 3).

Alloy	Time [h]	Concentration of metallic ions [mmol/cm ²]			
		Ti	Nb	Ta	Zr
Ti-Nb	2	9.1E-05 \pm 3.1E-06	2.4E-05 \pm 7.4E-06	0	0
	24	3.7E-04 \pm 4.0E-05	2.1E-04 \pm 2.1E-05	0	0
	48	6.5E-04 \pm 5.2E-06	2.9E-04 \pm 1.4E-05	0	0
	336	7.7E-04 \pm 4.2E-07	2.9E-04 \pm 7.5E-07	0	0
TNTZ	2	1.3E-05 \pm 6.3E-07	5.1E-06 \pm 6.5E-07	9.4E-07 \pm 5.5E-08	4.9E-07 \pm 1.2E-08
	24	8.4E-05 \pm 2.5E-06	4.1E-05 \pm 4.5E-06	5.7E-06 \pm 4.4E-07	3.7E-06 \pm 3.3E-07
	48	1.4E-04 \pm 4.0E-06	6.2E-05 \pm 1.7E-07	1.3E-05 \pm 1.7E-07	4.7E-06 \pm 2.8E-07
	336	2.6E-04 \pm 9.0E-06	8.4E-05 \pm 2.8E-07	1.6E-05 \pm 2.7E-07	6.5E-06 \pm 8.4E-07

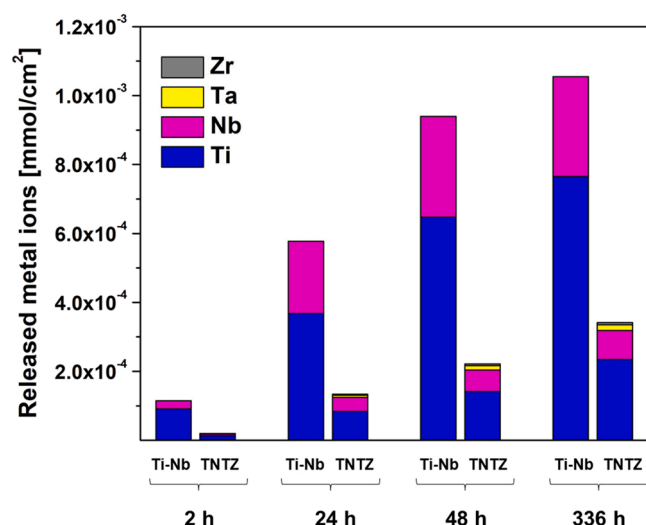


Fig. 4. Concentration of ions released into the PBS+H₂O₂ solution after different immersion times (average values).

immersion period (Table 3). Corrosion response is closely related to the topography, thickness and chemical composition of the oxide layers. In order to gain knowledge about the evolution of the oxide layers under inflammatory conditions, all of the features mentioned above were evaluated in the as-polished state, as well as after a prolonged immersion of 336 h in PBS+H₂O₂.

3.3. Oxide layers characteristics – topography

A quantitative AFM analysis showed that the level of surface roughness for the as-polished samples was virtually the same (for both Ti-Nb and TNTZ the largest difference between “peak” and “valleys” was

lower than 0.5 nm). It can therefore be assumed that all of the differences in surface topography observed after the immersion tests were related only to the interaction between the alloys’ surfaces and the solution. The AFM results did not demonstrate the presence of any microscopic cracks or other corrosion-induced damage. However, the interaction between the alloy surfaces and the H₂O₂ resulted in the formation of a nanoscale topography without any specific ordering (Fig. 5). Although the corrosion-induced changes are subtle in both alloys, the AFM analysis revealed that the surface topography was more stable in the case of the TNTZ alloy (Fig. 5). For the TNTZ, the largest difference between the “peaks” and “valleys” was less than 1.5 nm, while for the Ti-Nb it was c.a. 6 nm. Considering the fact that the interaction between H₂O₂ and the Ti surfaces resulted in Ti oxidation and a further repassivation of the more developed oxide layer, the AFM results supported the assumption that TNTZ is less prone to dissolution under simulated inflammation. This finding correlates with the conclusion drawn from the EIS and ICP-MS measurements.

3.4. Oxide layer characteristics – thickness and phase structure

The characterization of the surface topography was supplemented by an analysis of oxide layer thickness in the as-polished state (by AES) and after 336 h of immersion in PBS+H₂O₂ (by AES, and TEM). In AES studies, the border between the oxide layer and the alloy was assumed to be the point having approx. 66 % of the maximum oxygen value (Fig. 6). According to this criterion, the thickness of the air-formed passive layer formed on the Ti-Nb and TNTZ alloys did not exceed a dozen nanometers. AES measurements revealed that two weeks of immersion in the simulated inflammatory environment resulted in the substantial built-up of the oxidation products on the alloys’ surfaces (Fig. 6). Moreover, it was found that the layer of deposited oxides was approximately two times thicker for Ti-Nb alloy. Using spectroscopic techniques, one can only assess the order of magnitude of the thickness of the re-passivated film. Therefore, the thickness of the oxidation products zone, that

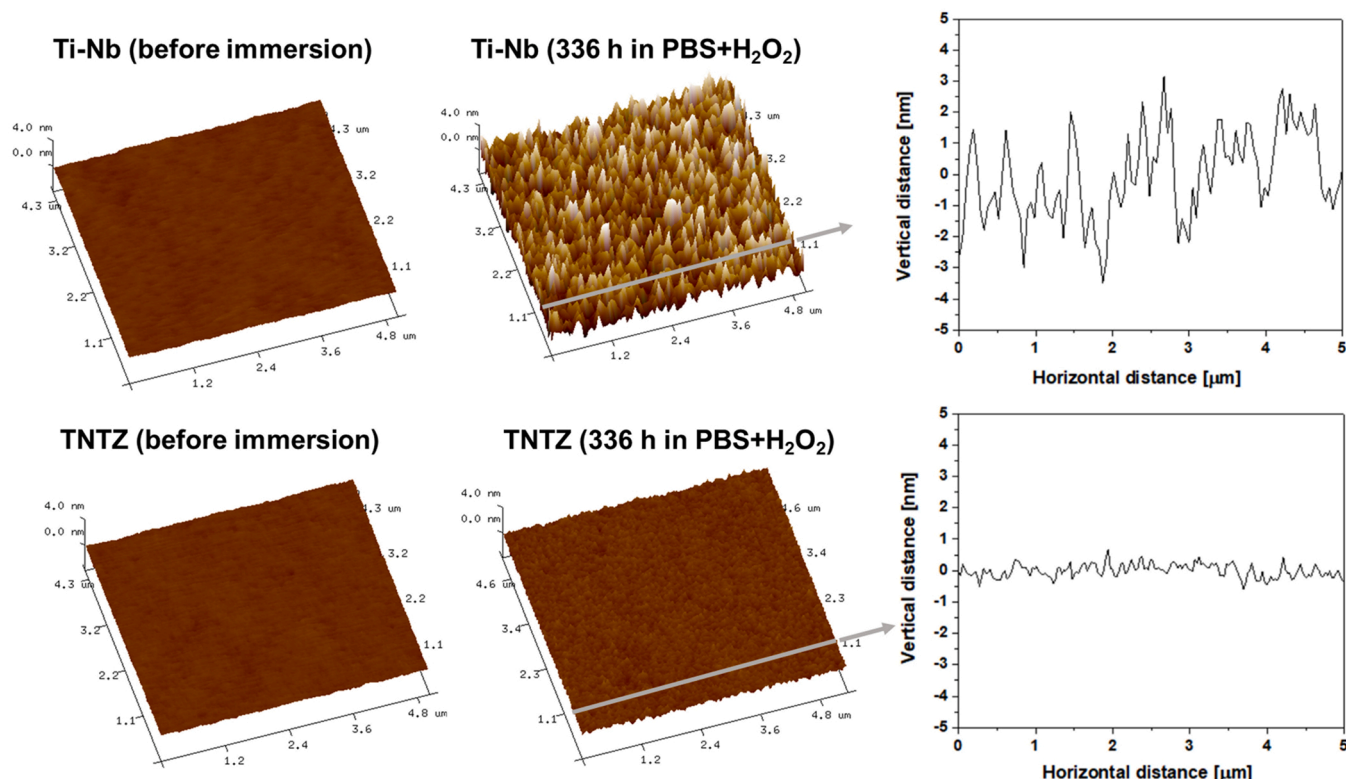


Fig. 5. Changes in the surface topography induced by 336 h of immersion in PBS+H₂O₂ (AFM studies).

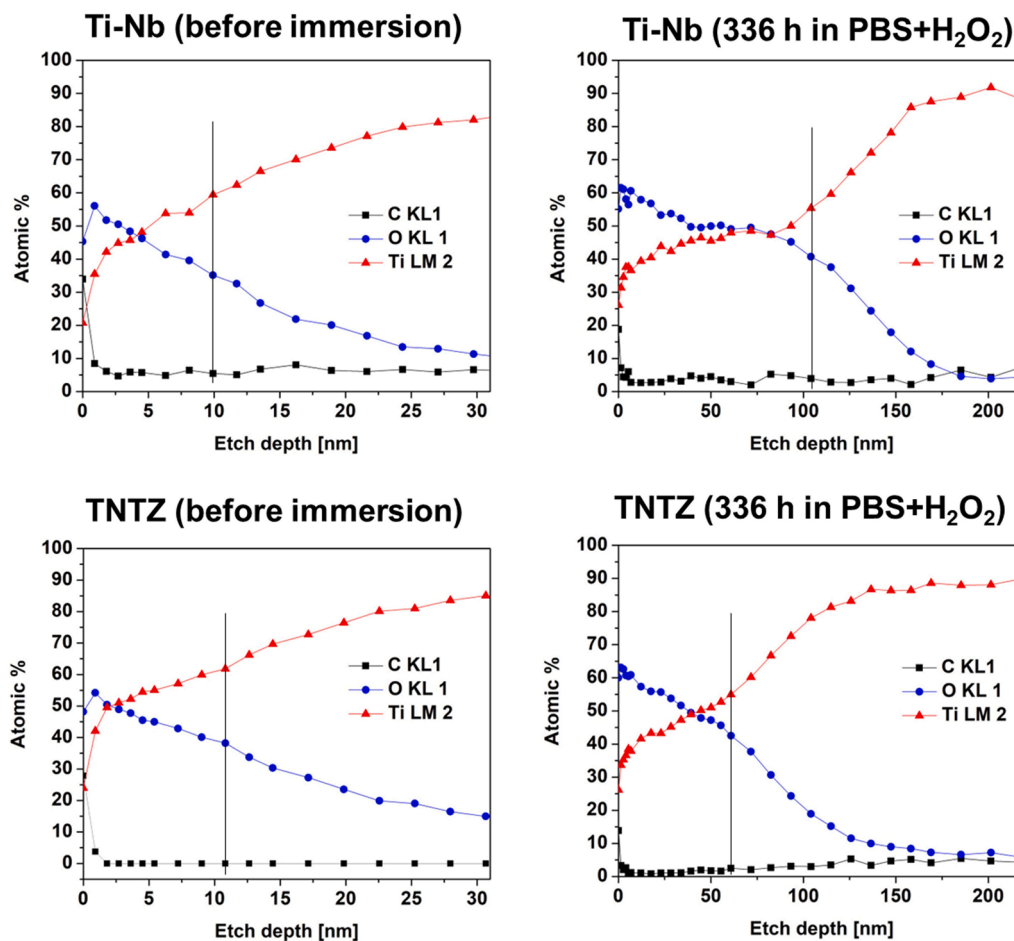


Fig. 6. Thickness of the air-formed passive layers and oxide corrosion products deposited during 336 h of immersion in PBS+H₂O₂ evaluated by AES studies (boundary between the oxide layer and metal is marked by vertical lines).

growth during the 336 h of alloys' immersion in PBS+H₂O₂ was additionally analyzed by TEM observations of FIB-lamellas that were prepared for the cross section of the samples. The microscopic observations revealed the presence of the compact and continuous oxide layer with approx. 5–10 nm in thickness (Fig. 7). Moreover, for both alloys the porous and non-continuous area of the oxidation products that were re-passivated on the alloys' surfaces can be distinguished. The high porosity of the re-passivated layer was confirmed by large number of gold particles that penetrated the corrosion products during sputtering of the protective gold layer in FIB. The thickness of re-passivated layer deposited on the Ti-Nb was about 30 nm, and on the TNTZ about 10 nm (Fig. 7). Another factor that could be important in terms of corrosion resistance is the phase structure of the oxide layer [58]. HR-TEM micrographs, performed at the boundary between the oxide layer and the substrate, indicated that the character of the oxide layer was amorphous. This observation was confirmed by the fast Fourier transforms (FFT) registered from the oxide area (Fig. 7).

3.5. Oxide layer characteristics – chemical composition

Knowledge about the evolution of the chemical composition of the oxide layers in the PBS+H₂O₂ was possible to gain by deconvoluting the HR-XPS spectra (Fig. 8, Fig. 9). Revealing the peaks from the metallic elements for the as-polished samples confirmed the nanometric thickness of the passive layers formed on their surfaces (Fig. 8, Fig. 9). For both as-polished alloys, different Ti (TiO, Ti₂O₃, TiO₂) as well as Nb oxides (NbO, NbO₂, Nb₂O₅; Ti-Nb; NbO, Nb₂O₅; TNTZ) were detected within the oxide layers formed on their surfaces (Fig. 10). Additionally,

for the TNTZ alloy, the HR-XPS spectra revealed peaks from Ta and Zr at their highest oxidation states (Ta₂O₅ and ZrO₂, respectively). The absence of Ta and Zr sub-oxides could be related to their higher tendency to oxidize compared with Ti and Nb, which was confirmed by the thermodynamic calculations [59]. For both the Ti-Nb and TNTZ alloys, two weeks of exposure in PBS+H₂O₂ produced noticeable changes in the stoichiometry of the oxide layers. Firstly, oxidation of Ti and Nb sub-oxides took place, and for both alloys the oxide layer was composed only from alloying elements at the highest oxidation states (TiO₂, Nb₂O₅, Ta₂O₅, and ZrO₂) (Fig. 10). The content of TiO₂ and Nb₂O₅ detected for the Ti-Nb alloy was approximately proportional to the composition of the substrate. In the case of the TNTZ alloy, a substantial increase in ZrO₂ was observed. The content of ZrO₂ in the surface went up from about 4.0–17.5%. (Fig. 10). Considering the fact that both β -phase alloys demonstrated the same type of microstructure (virtually the same average grain size and grain size distribution) and very similar surface topographies in the as-polished state, the differences in the chemical composition of the compact oxide layers should be responsible for the different corrosion behavior of the Ti-Nb and TNTZ alloys.

4. Discussion

Currently, relatively new groups of Ti β -phase binary Ti-Nb and quaternary Ti-Nb-Ta-Zr (TNTZ) alloys are attracting a lot of scientific interest because of their potential application in long-lasting implantology [45,60–62]. This is mainly due to their unique mechanical properties and simultaneous lack of potentially harmful alloying elements. However, the success of an implantation is also related to the

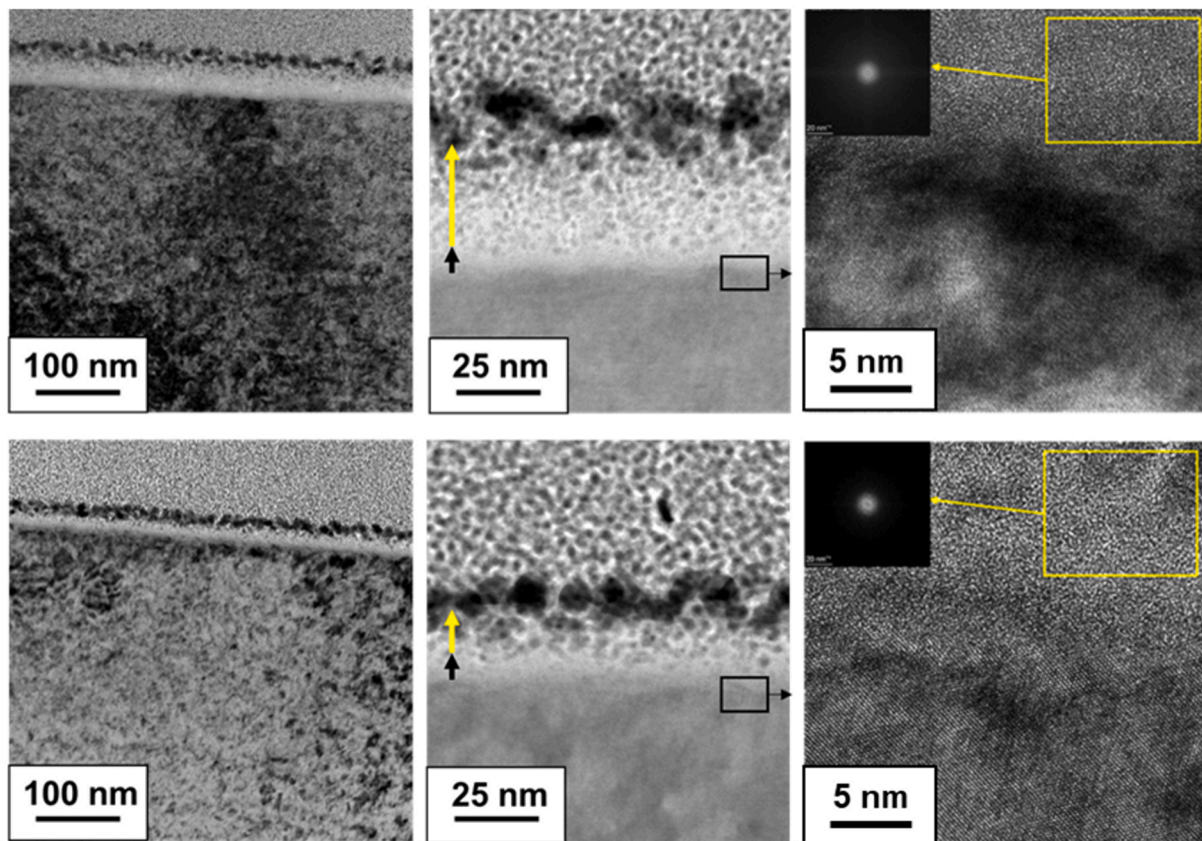


Fig. 7. Thickness and phase structure of the oxide layers evaluated based on TEM and HR-TEM observations of the surfaces cross-sections performed after 336 h of immersion in PBS+H₂O₂ (compact film is marked by black arrow and the layer of corrosion products by yellow arrow). (For interpretation of the references to color in this figure legend, the reader is referred to the web version of this article.)

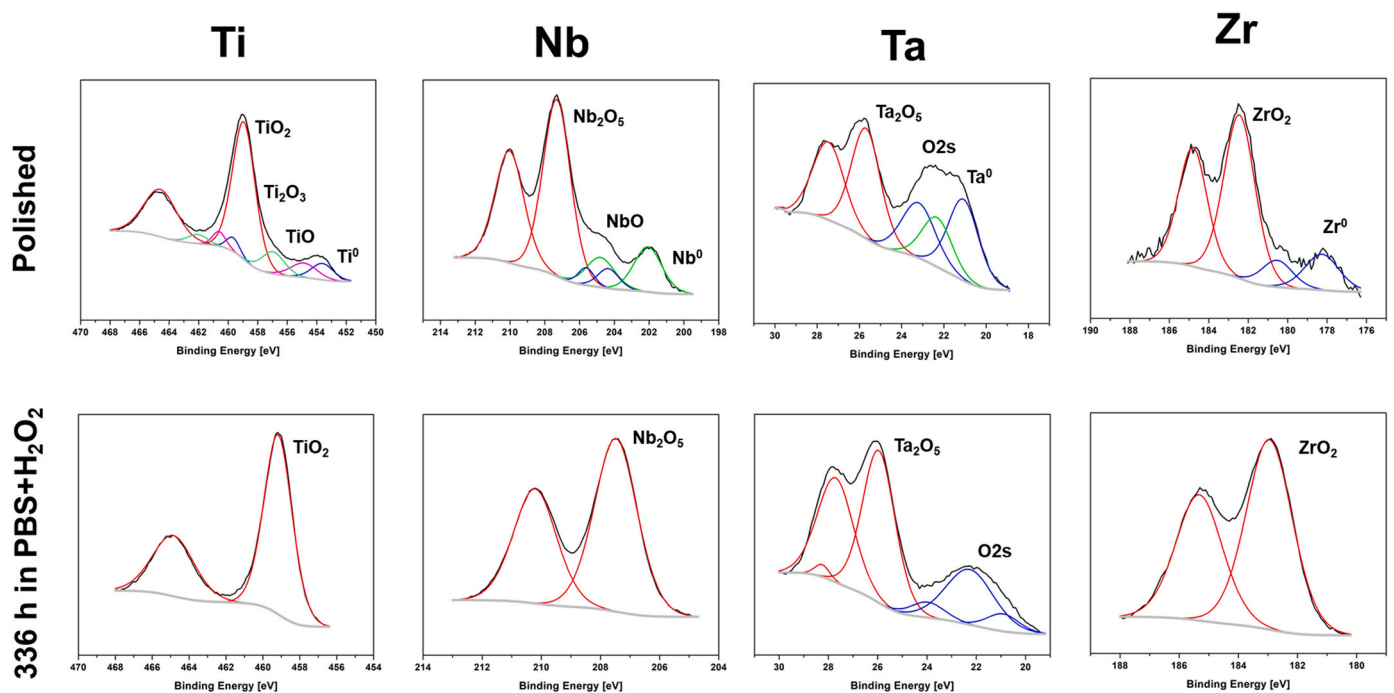


Fig. 8. HR-XPS spectra recorded for TNTZ alloy before and after 336 h of immersion in PBS+H₂O₂.

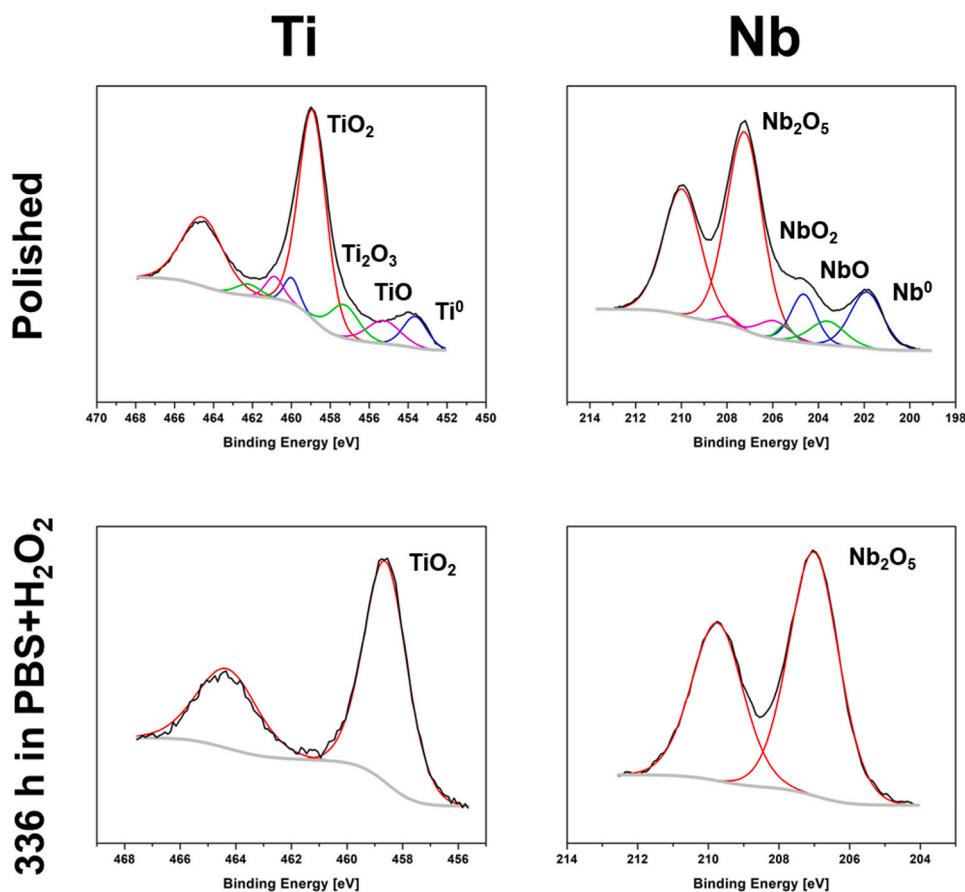


Fig. 9. HR-XPS spectra recorded for Ti-Nb alloy before and after 336 h of immersion in PBS+H₂O₂.

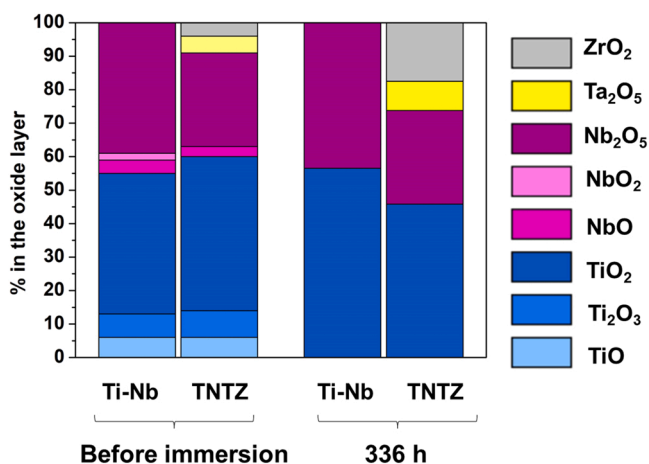


Fig. 10. Changes in the chemical composition of the surface induced by 336 h of immersion in PBS+H₂O₂.

surface properties of the materials used, such as their corrosion resistance. This study compared the corrosion resistance of Ti-Nb and Ti-Nb-Ta-Zr under simulated inflammatory conditions that resembled the peri-implant environment more realistically than the standard solutions used for testing biomaterials. The overall results revealed that quaternary the TNTZ alloy exhibited significantly better corrosion resistance than the Ti-Nb alloy ($p < 0.01$). Both the EIS and the ICP-MS tests confirmed the TNTZ's superior corrosion properties, during initial exposure in PBS+H₂O₂ (2 h) and after prolonged solution immersion times (24 h, 48 h, 336 h). Better corrosion resistance of TNTZ was

reflected by the larger values of R_{ox} and by the lower amount of metal ions released to the PBS+H₂O₂. It has to be added that for both alloys' the R_{ox} value increased after prolonged immersion in the solution, which indicate on the enhancement of their corrosion resistance. Contrary to the R_{ox} values, C_{eff} designated from the EIS data did not change during the whole immersion period (considering the standard deviation values – Table 2). This indicates that thickness of the compact oxide layer, which contributes to the high corrosion resistance, remains stable during the whole exposure period in PBS+H₂O₂. Generally, when the R_{ox} value increasing, decrease of C_{eff} value can be observed [63,64]. At the early immersion stages, R_{ox} was the lowest because H₂O₂-rich solution enforces alloys' oxidation. Titanium oxide (and also complex oxides that are formed on TNTZ and Ti-Nb surfaces) can be classified as n-type semiconductor and chemical reactions are taking place at the substrate/compact oxide interface. Then, metal ions are transported across the film, and can remain in the solution (as was found based on ICP-MS) or can be further re-deposited on the surface in the form of oxides (as was shown in TEM micrographs). Hydrogen peroxide is unstable compound, so after longer immersion time its decomposition taking place, and the solution is losing its oxidation power. Consequently, the resistance of the compact oxide layer increases, but its thickness remains unchanged. The lack of growth of the compact oxide layer in PBS+H₂O₂ was confirmed also based on the post-immersion TEM observations which revealed that its thickness was similar to those assessed for the native passive layer based on the AES studies (Fig. 6, Fig. 7). For both samples thickness of the compact oxide film after EIS tests did not exceed 10 nm. However, differences were found in the thickness of the corrosion products layer, which was more than a twice as thick for Ti-Nb than for TNTZ alloy. Less intensive increase in the thickness of the layer of corrosion products after prolonged immersion in PBS+H₂O₂ confirmed the higher stability of the TNTZ surface under simulated

inflammation, which was reflected by the larger R_{ox} values and lower amount of metal ions released to the solution.

The differences observed in the protective properties of the oxide layers formed on the Ti-based alloys tested could be related to the following factors: (i) the different chemical composition, and (ii) distinct microstructural features of the substrates. It is well known that grain boundaries act as privileged sites for chemical reactions, and consequently, a high number of these defects could enhance both dissolution and further repassivation processes. The similar microstructure and grain size of the Ti-Nb and TNTZ alloys, achieved by varying the heat-treatment parameters, permitted the inference that the beneficial corrosion behavior of the TNTZ alloy was strictly related to its more complex chemical composition. Previous EIS data indicated that TNTZ alloy is less likely to react chemically with H_2O_2 than is the widely used biomedical CP-Ti [7]. In accordance with the proposed hypothesis, this effect could be explained by the presence of alloying elements having higher valences than Ti. The passive layer that is air-formed on the Ti surface contains a certain amount of oxygen vacancies whose origin is related to the presence of Ti oxides at lower oxidation states than TiO_2 [41]. Literature data have shown that the highest protectiveness of an air-formed oxide layer on Ti and its alloys, is usually achieved in case of the lowest amount of TiO and Ti_2O_3 [65,66]. It is believed that the presence of Nb^{5+} and/or Ta^{5+} cations within the passive layer could compensate for the existence of oxygen vacancies [67,68]. For this reason, in previous studies binary Ti-Nb alloys were also found to be more corrosion resistant than CP-Ti [69,70]. However, it should be added that, in those cases, this beneficial effect was visible in acidic solutions enriched with fluorides that simulated the conditions in the oral cavity. Similar findings were also reported for the multicomponent, microcrystalline TNTZ alloy, which demonstrates better initial corrosion resistance in fluoridated saliva than CP-Ti [11]. These results permit the conclusion that the presence of Nb_2O_5 and/or Ta_2O_5 in the oxide layer formed on Ti-based alloys impedes Ti dissolution in the conditions that facilitate their local corrosion. Nevertheless, the results presented in this study revealed that TNTZ demonstrates significantly higher corrosion resistance in $PBS+H_2O_2$ compared with Ti-Nb, despite having a similar content of alloying elements with higher valences than Ti. Therefore, the effect of Nb and Ta on corrosion resistance in highly oxidizing conditions is not straightforward, and the presence of alloying elements with higher valences than Ti cannot simply explain the beneficial corrosion behavior observed for TNTZ. While in other works corrosion resistance was evaluated based on the oxygen vacancies concept, our manuscript documented increased corrosion resistance of TNTZ in the $PBS+H_2O_2$ solution based on the combined experimental evidence that includes electrochemical (EIS), ion-release (ICP-MS), and microscopic analysis (AFM, TEM).

The surface chemical composition, and its corrosion-induced changes provided increased understanding for the better protection achieved by the oxide film formed on TNTZ. The XPS studies demonstrated that additionally to Ti and Nb oxides that were found on the Ti-Nb surface, native compact film formed on TNTZ surface contains also Ta and Zr oxides. After 336 h of TNTZ immersion in $PBS+H_2O_2$, a substantial increase in the ZrO_2 content was revealed. This could be explained by considering the energy necessary for oxide formation, which is lower for Zr than for Ti and Nb [59]. According to Taylor et al. [59], the calculated value of that energy is similar for Zr and Ta. However, cohesive energy, which acts as an indicator of the metal-metal bond strengths, is significantly higher in Ta, meaning that the oxidation of Zr and the formation of Zr oxides should be energetically favorable in the highly oxidizing conditions that are found under inflammatory conditions. An enrichment of the surface in ZrO_2 was suggested as a possible reason for the better corrosion properties in $PBS+H_2O_2$ reported for the binary Ti-Zr biomedical alloy (compared with the conventional CP-Ti) [71]. In this work it was found that, contrary to titanium oxides, ZrO_2 is resistant to dissolution induced by H_2O_2 . Although ZrO_2 does not undergo a chemical reaction with H_2O_2 ,

its surface provides catalytic support for the decomposition of H_2O_2 [72]. Presence of the ZrO_2 in the oxide layer formed on TNTZ alloy might cause a faster reduction in the solution's oxidizing power in the case of TNTZ, which could in turn be the reason of faster growth of the R_{ox} value with the immersion time than in the case of the Ti-Nb alloy. Both high resistance to dissolution and the catalytic character of ZrO_2 could be responsible for the suppressed release of metal ions. In turn, the lower content of metal ions in the solution resulted in thinner layer of oxide products that were re-deposited on the TNTZ surface after corrosion process. The origin of the thicker oxide layer observed for the binary alloy could be related to the larger amount of released metal ions that were able to take part in the formation of the re-passivated layer of corrosion products, in the form of oxides, in the case of prolonged immersion in $PBS+H_2O_2$.

Based on presented results supported by literature data, we hypothesize that Zr could play important role in tailoring TNTZ corrosion resistance under simulated inflammatory conditions. However, the investigation performed in this study cannot answer whether the observed behavior of the TNTZ alloy is governed only by the presence of Zr or by the combined effect of Zr and other alloying elements with higher valences. For this reason, it would be worth comparing the corrosion behavior of TNTZ with a binary alloy having similar Zr content (e.g. Ti-5Zr). Nevertheless, it must be considered that the TNTZ and Ti-Zr alloys have different phase compositions, owing to the fact that Zr is not a strong β -phase stabilizer in Ti. Moreover, the experiments described in this study do not exclude the important role of Ta in tailoring TNTZ's corrosion behavior in $PBS+H_2O_2$. However, in the case of binary Ti-Ta alloys, the almost single β phase can only be obtained at a high content of Ta [73], and so comparing TNTZ with a binary alloy of similar Ta content would not provide information about the separate role of Ta, owing to the differences in the phase structures of the tested alloys. Finally, it have to be mentioned that in this study the effect of chemical composition on the corrosion behavior under simulated inflammation was studied for alloys with the microstructures composed from equiaxed and defect-free micrometric grains. Future studies are needed to gain the knowledge about the combined influence of biocompatible alloying elements and the alloys' density of defects of crystallographic structure (e.g. grain boundaries, dislocations), which is related to the selected path of manufacturing process.

5. Conclusions

In this work, the time-dependent corrosion resistance of biomedical titanium β -phase alloys of reduced stiffness (Ti-Nb and Ti-Nb-Ta-Zr: TNTZ) was compared in a solution simulating post-operative inflammatory conditions ($PBS+H_2O_2$). Developing alloys having the same type of microstructure and virtually the same grain size permitted us to understand the separate role of chemical composition on corrosion behavior. The experimental results led to the following conclusions:

- Ti-Nb-Ta-Zr (TNTZ) demonstrated significantly higher corrosion resistance in $PBS+H_2O_2$ solution than the Ti-Nb alloy did, despite a similar content of alloying elements with higher valences (β -phase stabilizers) than those of Ti (Ti-Nb: 45 wt% Nb, TNTZ: 29 wt% Nb+13 wt% Ta).
- Better corrosion resistance of TNTZ compared to Ti-Nb was confirmed by both higher values of oxide layer resistance and lower concentration of released metal ions to the $PBS+H_2O_2$ after initial (2 h, 24 h, 48 h) as well as prolong immersion (336 h) in the solution.
- After prolong exposure in the simulated inflammatory environment, re-passivated layer of the oxidation products formed on the TNTZ surface was more than a double as thin as those formed on Ti-Nb alloy. Moreover, TNTZ immersion in $PBS+H_2O_2$ resulted in lower development of surface topography compared to Ti-Nb alloy. Described observation indicate that the corrosion process and further

built-up of the corrosion products was less intensive for TNTZ alloy. Thereby, results of surface analysis correlates with findings derived from electrochemical and ion-release tests.

- Surface chemical composition analysis revealed that 336 h of TNTZ immersion in PBS+H₂O₂ resulted in the substantial enrichment in the Zr oxide. The content of ZrO₂ in the surface exceeded 17.5 % despite less than 5 wt% of metallic Zr in the TNTZ substrate. Overall results allow to conclude that amongst other chemical elements in TNTZ, Zr oxidize preferentially and does not show a tendency to interact with H₂O₂.
- Ti-Nb alloy demonstrated suppressed rate of R_{ox} growth with immersion time compared to TNTZ during exposure in PBS+H₂O₂. Although Nb is known to enhance Ti resistance to local corrosion, overall results presented in this work allow to exclude its beneficial role in case of corrosion behavior under simulated inflammatory conditions. Considering the fact that the interaction between a biomaterial and the human body involves two-way positive feedback, both of the above findings are valuable in terms of corrosion behavior of Ti β-phase alloys in the real peri-implant inflammatory environment.

CRedit authorship contribution statement

Agata Sotniczuk: Conceptualization, Methodology, Investigation, Project administration, Funding acquisition, Writing – original draft. **Jeremy L. Gilbert:** Supervision, Methodology, Writing – review & editing. **Yangping Liu:** Methodology, Investigation, Writing – review & editing. **Magdalena Matczuk:** Investigation, Writing – review & editing. **Witold Chromiński:** Investigation, Writing – review & editing. **Damian Kalita:** Investigation, Writing – review & editing. **Marcin Pisarek:** Investigation, Writing – review & editing. **Halina Garbacz:** Supervision, Writing – review & editing, Funding acquisition.

Declaration of Competing Interest

The authors declare the following financial interests/personal relationships which may be considered as potential competing interests: Jeremy L. Gilbert: Consultant for Stryker Orthopedics, Zimmer Biomet, Smith and Nephew, Omniflife Sciences, and DePuy Synthes. Research support to Clemson from Bayer Inc, and DePuy Synthes. Editor-in-Chief of Journal of Biomedical Materials Research – Part B: Applied Biomaterials, J Wiley and Sons, and member of the council of the Society For Biomaterials.

Data availability

Data will be made available on request.

Acknowledgements

This research was supported financially by the National Science Centre, Poland under the grant PRELUDIUM 15 [2018/29/N/ST8/02306].

The microstructure of the TNTZ alloy was developed and characterized within a project funded by POB “Technologie Materiałowe” of Warsaw University of Technology within the Excellence Initiative: Research University (IDUB) Programme.

FIB preparation was funded by the European Union Horizon 2020 Research and Innovation Program under Grant Agreement No. 857470 and from the European Regional Development Fund via Foundation for Polish Science International Research Agenda PLUS Program Grant No. MAB PLUS/2018/8.

References

- [1] N. Hu, L. Xie, Q. Liao, A. Gao, Y. Zheng, H. Pan, L. Tong, D. Yang, N. Gao, M. J. Starink, A more defective substrate leads to a less defective passive layer: enhancing the mechanical strength, corrosion resistance and anti-inflammatory response of the low-modulus Ti-45Nb alloy by grain refinement, *Acta Biomater.* 126 (2021) 524–536, <https://doi.org/10.1016/j.actbio.2021.02.045>.
- [2] S.S. Sidhu, H. Singh, M.A.-H. Gepreel, A review on alloy design, biological response, and strengthening of β-titanium alloys as biomaterials, *Mater. Sci. Eng. C* 121 (2021), 111661, <https://doi.org/10.1016/j.msec.2020.111661>.
- [3] C.A.E. Claros, L.C. Campanelli, A.M.J. Junior, J.-C. Leprêtre, C. Bolfarini, V. Roche, Corrosion behaviour of biomedical β-titanium alloys with the surface-modified by chemical etching and electrochemical methods, *Corros. Sci.* 188 (2021), 109544, <https://doi.org/10.1016/j.corsci.2021.109544>.
- [4] S. Bahl, S. Suwas, K. Chatterjee, Comprehensive review on alloy design, processing, and performance of β Titanium alloys as biomedical materials, *Int. Mater. Rev.* 66 (2020) 1–26, <https://doi.org/10.1080/09506608.2020.1735829>.
- [5] L.-C. Zhang, L.-Y. Chen, L. Wang, Surface modification of titanium and titanium alloys: technologies, developments, and future interests, *Adv. Eng. Mater.* 22 (2020), 1901258, <https://doi.org/10.1002/adem.201901258>.
- [6] M. Kaur, K. Singh, Review on titanium and titanium based alloys as biomaterials for orthopaedic applications, *Mater. Sci. Eng. C* 102 (2019) 844–862, <https://doi.org/10.1016/j.msec.2019.04.064>.
- [7] A. Sotniczuk, D. Kuczyńska-Zemla, P. Kwaśniak, M. Thomas, H. Garbacz, Corrosion behavior of Ti-29Nb-13Ta-4.6Zr and commercially pure Ti under simulated inflammatory conditions – comparative effect of grain refinement and non-toxic β phase stabilizers, *Electrochim. Acta* 312 (2019) 369–379, <https://doi.org/10.1016/j.electacta.2019.04.138>.
- [8] L. Kuncická, R. Kocich, T.C. Lowe, Advances in metals and alloys for joint replacement, *Prog. Mater. Sci.* 88 (2017) 232–280, <https://doi.org/10.1016/j.pmatsci.2017.04.002>.
- [9] J. Nagels, M. Stokdijk, P.M. Rozing, Stress shielding and bone resorption in shoulder arthroplasty, *J. Shoulder Elb. Surg.* 12 (2003) 35–39, <https://doi.org/10.1067/mse.2003.22>.
- [10] D. Kuroda, M. Niinomi, M. Morinaga, Y. Kato, T. Yashiro, Design and mechanical properties of new β type titanium alloys for implant materials, *Mater. Sci. Eng. A* 243 (1998) 244–249, [https://doi.org/10.1016/S0921-5093\(97\)00808-3](https://doi.org/10.1016/S0921-5093(97)00808-3).
- [11] A. Sotniczuk, K. Majchrowicz, D. Kuczyńska-Zemla, M. Pisarek, B. Adamczyk-Cieślak, H. Garbacz, Surface properties and mechanical performance of Ti-based dental materials: comparative effect of valve alloying elements and structural defects, *Metall. Mater. Trans. A* 53 (2021) 1–15, <https://doi.org/10.1007/s11661-021-06515-y>.
- [12] Y.L. Hao, R. Yang, M. Niinomi, D. Kuroda, Y.L. Zhou, K. Fukunaga, A. Suzuki, Aging response of the Young's modulus and mechanical properties of Ti-29Nb-13Ta-4.6 Zr for biomedical applications, *Metall. Mater. Trans. A* 34 (2003) 1007–1012, <https://doi.org/10.1007/s11661-002-0299-7>.
- [13] M. Geetha, A.K. Singh, R. Asokamani, A.K. Gogia, Ti based biomaterials, the ultimate choice for orthopaedic implants – a review, *Prog. Mater. Sci.* 54 (2009) 397–425, <https://doi.org/10.1016/j.pmatsci.2008.06.004>.
- [14] Z. Li, B. Zheng, Y. Wang, T. Topping, Y. Zhou, R.Z. Valiev, A. Shan, E.J. Lavernia, Ultrafine-grained Ti-Nb-Ta-Zr alloy produced by ECAP at room temperature, *J. Mater. Sci.* 49 (2014) 6656–6666, <https://doi.org/10.1007/s10853-014-8337-6>.
- [15] H. Yilmazer, M. Şen, M. Niinomi, M. Nakai, L. Huihong, K. Cho, Y. Todaka, H. Shiku, T. Matsue, Developing biomedical nano-grained β-type titanium alloys using high pressure torsion for improved cell adherence, *RSC Adv.* 6 (2016) 7426–7430, <https://doi.org/10.1039/C5RA23454A>.
- [16] F. Haftlang, A. Zarei-Hanzaki, H.R. Abedi, M.A. Kalaei, Tribological performance and electrochemical behavior of Ti-29Nb-14Ta-4.5 Zr alloy in simulated physiological solution, *Adv. Eng. Mater.* 22 (2020), 1900758, <https://doi.org/10.1002/adem.201900758>.
- [17] D. Kuczyńska-Zemla, E. Kjińska-Gawrońska, A. Chlanda, A. Sotniczuk, M. Pisarek, K. Topolski, W. Swieszkowski, H. Garbacz, Biological properties of a novel β-Ti alloy with a low Young's modulus subjected to cold rolling, *Appl. Surf. Sci.* 511 (2020), 145523, <https://doi.org/10.1016/j.apsusc.2020.145523>.
- [18] V. Raman, S. Nagarajan, N. Rajendran, Electrochemical impedance spectroscopic characterisation of passive film formed over β Ti-29Nb-13Ta-4.6 Zr alloy, *Electrochem. Commun.* 8 (2006) 1309–1314, <https://doi.org/10.1016/j.elecom.2006.06.004>.
- [19] A.C. Bărbînță, D. Mareci, R. Chelariu, G. Bolat, C. Munteanu, K. Cho, M. Niinomi, The estimation of corrosion behavior of new TiNbTaZr alloys for biomedical applications, *Mater. Corros.* 65 (2014) 1017–1023, <https://doi.org/10.1002/maco.201307294>.
- [20] M. Prestat, D. Thierry, Corrosion of titanium under simulated inflammation conditions: clinical context and in vitro investigations, *Acta Biomater.* 136 (2021) 72–87, <https://doi.org/10.1016/j.actbio.2021.10.002>.
- [21] A. Sotniczuk, W. Chromiński, B. Adamczyk-Cieślak, M. Pisarek, H. Garbacz, Corrosion behaviour of biomedical Ti under simulated inflammation: exploring the relevance of grain refinement and crystallographic texture, *Corros. Sci.* 200 (2022), 110238, <https://doi.org/10.1016/j.corsci.2022.110238>.
- [22] J.L. Gilbert, G.W. Kubacki, Oxidative stress, inflammation, and the corrosion of metallic biomaterials: corrosion causes biology and biology causes corrosion, in: *Oxidative Stress Biomater.*, Elsevier, 2016, pp. 59–88, <https://doi.org/10.1016/B978-0-12-803269-5.00003-6>.
- [23] S. Amin Yavari, S.M. Castenmiller, J.A.G. van Strijp, M. Croes, Combating implant infections: shifting focus from bacteria to host, *Adv. Mater.* 32 (2020), 2002962, <https://doi.org/10.1002/adma.2002962>.

- [24] G. Mabileau, S. Bourdon, M.L. Joly-Guillou, R. Filmon, M.F. Baslé, D. Chappard, Influence of fluoride, hydrogen peroxide and lactic acid on the corrosion resistance of commercially pure titanium, *Acta Biomater.* 2 (2006) 121–129, <https://doi.org/10.1016/j.actbio.2005.09.004>.
- [25] A. Fonseca-García, J. Pérez-Alvarez, C.C. Barrera, J.C. Medina, A. Almaguer-Flores, R.B. Sánchez, S.E. Rodil, The effect of simulated inflammatory conditions on the surface properties of titanium and stainless steel and their importance as biomaterials, *Mater. Sci. Eng. C* 66 (2016) 119–129, <https://doi.org/10.1016/j.msec.2016.04.035>.
- [26] M. Prestat, F. Vucko, L. Holzer, D. Thierry, Microstructural aspects of Ti6Al4V degradation in H₂O₂-containing phosphate buffered saline, *Corros. Sci.* 190 (2021), 109640, <https://doi.org/10.1016/j.corsci.2021.109640>.
- [27] C. Fonseca, M. Barbosa, Corrosion behaviour of titanium in biofluids containing H₂O₂ studied by electrochemical impedance spectroscopy, *Corros. Sci.* 43 (2001) 547–559, [https://doi.org/10.1016/S0010-938X\(00\)00107-4](https://doi.org/10.1016/S0010-938X(00)00107-4).
- [28] J. Pan, D. Thierry, C. Leygraf, Electrochemical and XPS studies of titanium for biomaterial applications with respect to the effect of hydrogen peroxide, *J. Biomed. Mater. Res.* 28 (1994) 113–122, [https://doi.org/10.1016/0142-9612\(89\)90019-7](https://doi.org/10.1016/0142-9612(89)90019-7).
- [29] P. Tengvall, I. Lundström, L. Sjöqvist, H. Elwing, L.M. Bjursten, Titanium-hydrogen peroxide interaction: model studies of the influence of the inflammatory response on titanium implants, *Biomaterials* 10 (1989) 166–175, [https://doi.org/10.1016/0142-9612\(89\)90019-7](https://doi.org/10.1016/0142-9612(89)90019-7).
- [30] E. Brooks, M. Tobias, K. Krautsak, M. Ehrensberger, The influence of cathodic polarization and simulated inflammation on titanium electrochemistry, *J. Biomed. Mater. Res. Part B Appl. Biomater.* 102 (2014) 1445–1453, <https://doi.org/10.1002/jbm.b.33123>.
- [31] A. Mace, J. Gilbert, A mass balance analysis of the tribocorrosion process of titanium alloys using a single micro-asperity: voltage and solution effects on plastic deformation, oxide repassivation, and ion dissolution, *J. Mech. Behav. Biomed. Mater.* 136 (2022), 105531, <https://doi.org/10.1016/j.jmbmm.2022.105531>.
- [32] Y. Liu, D. Zhu, J.L. Gilbert, Sub-nano to nanometer wear and tribocorrosion of titanium oxide-metal surfaces by in situ atomic force microscopy, *Acta Biomater.* 126 (2021) 477–484, <https://doi.org/10.1016/j.actbio.2021.03.049>.
- [33] J.L. Gilbert, S. Sivan, Y. Liu, S.B. Kocagöz, C.M. Armholt, S.M. Kurtz, Direct in vivo inflammatory cell-induced corrosion of CoCrMo alloy orthopedic implant surfaces, *J. Biomed. Mater. Res. Part A* 103 (2015) 211–223, <https://doi.org/10.1002/jbm.a.35165>.
- [34] F. Yu, O. Addison, A.J. Davenport, A synergistic effect of albumin and H₂O₂ accelerates corrosion of Ti6Al4V, *Acta Biomater.* 26 (2015) 355–365, <https://doi.org/10.1016/j.actbio.2015.07.046>.
- [35] M.A. Kurtz, P. Khullar, J.L. Gilbert, Cathodic activation and inflammatory species are critical to simulating in vivo Ti-6Al-4V selective dissolution, *Acta Biomater.* 149 (2022) 399–409, <https://doi.org/10.1016/j.actbio.2022.07.020>.
- [36] S. Balachandran, Z. Zachariah, A. Fischer, D. Mayweg, M.A. Wimmer, D. Raabe, M. Herbig, Atomic scale origin of metal ion release from hip implant taper junctions, *Adv. Sci.* 7 (2020), 1903008, <https://doi.org/10.1002/adv.201903008>.
- [37] J. Qi, D. Guan, J. Nutter, B. Wang, W.M. Rainforth, Insights into tribofilm formation on Ti-⁶V-⁴Al in a bioactive environment: correlation between surface modification and micro-mechanical properties, *Acta Biomater.* 141 (2022) 466–480, <https://doi.org/10.1016/j.actbio.2022.01.027>.
- [38] A. Mace, J.L. Gilbert, Micro asperity-based fretting corrosion of CoCrMo, Ti-6Al-4V, and 316 L SS: assessment of an electrochemical and micro-mechanical model, *Tribol. Int.* 180 (2023), 108222, <https://doi.org/10.1016/j.triboint.2023.108222>.
- [39] D.R. Biju Kumar, S. Salunkhe, G. Zheng, M. Barba, D.J. Hall, R. Pourzal, M. T. Mathew, Wear particles induce a new macrophage phenotype with the potential to accelerate material corrosion within total hip replacement interfaces, *Acta Biomater.* 101 (2020) 586–597, <https://doi.org/10.1016/j.actbio.2019.10.039>.
- [40] J.L. Gilbert, Metallic degradation and the biological environment, in: *Biomater. Sci., Elsevier*, 2020, pp. 941–954, <https://doi.org/10.1016/B978-0-12-816137-1.00063-5>.
- [41] M. Metikos-Huković, A. Kwokal, J. Piljac, The influence of niobium and vanadium on passivity of titanium-based implants in physiological solution, *Biomaterials* 24 (2003) 3765–3775, [https://doi.org/10.1016/S0142-9612\(03\)00252-7](https://doi.org/10.1016/S0142-9612(03)00252-7).
- [42] R. Schmidt, A. Gebert, M. Schumacher, V. Hoffmann, A. Voss, S. Pilz, M. Uhlemann, A. Lode, M. Gelinsky, Electrodeposition of Sr-substituted hydroxyapatite on low modulus beta-type Ti-45Nb and effect on in vitro Sr release and cell response, *Mater. Sci. Eng. C* 108 (2020), 110425, <https://doi.org/10.1016/j.msec.2019.110425>.
- [43] I. Cvijović-Alagić, S. Laketić, J. Bajat, A. Hohenwarter, M. Rakin, Grain refinement effect on the Ti-45Nb alloy electrochemical behavior in simulated physiological solution, *Surf. Coat. Technol.* 423 (2021), 127609, <https://doi.org/10.1016/j.surfcoat.2021.127609>.
- [44] K. Ozaltın, W. Chrominski, M. Kulczyk, A. Panigrahi, J. Horky, M. Zehetbauer, M. Lewandowska, Enhancement of mechanical properties of biocompatible Ti-45Nb alloy by hydrostatic extrusion, *J. Mater. Sci.* 49 (2014) 6930–6936, <https://doi.org/10.1007/s10853-014-8397-7>.
- [45] L.A. Alberta, J. Vishnu, A. Hariharan, S. Pilz, A. Gebert, M. Calin, Novel low modulus beta-type Ti-Nb alloys by gallium and copper minor additions for antibacterial implant applications, *J. Mater. Res. Technol.* 20 (2022) 3306–3322, <https://doi.org/10.1016/j.jmrt.2022.08.111>.
- [46] I. Caha, A.C. Alves, P.A.B. Kuroda, C.R. Grandini, A.M.P. Pinto, L.A. Rocha, F. Toptan, Degradation behavior of Ti-Nb alloys: corrosion behavior through 21 days of immersion and tribocorrosion behavior against alumina, *Corros. Sci.* 167 (2020), 108488, <https://doi.org/10.1016/j.corsci.2020.108488>.
- [47] A. Panigrahi, B. Sulkowski, T. Waitz, K. Ozaltın, W. Chrominski, A. Pukenas, J. Horky, M. Lewandowska, W. Skrotzki, M. Zehetbauer, Mechanical properties, structural and texture evolution of biocompatible Ti-45Nb alloy processed by severe plastic deformation, *J. Mech. Behav. Biomed. Mater.* 62 (2016) 93–105, <https://doi.org/10.1016/j.jmbmm.2016.04.042>.
- [48] J. Wojcieszek, J. Jiménez-Lamana, L. Ruzik, M. Asztemborska, M. Jarosz, J. Szpunar, Characterization of TiO₂ NPs in radish (*Raphanus sativus* L.) by single-particle ICP-QQQ-MS, *Front. Environ. Sci.* 8 (2020) 100, <https://doi.org/10.3389/fenvs.2020.00100>.
- [49] J. Tang, H. Luo, Y. Qi, P. Xu, J. Lv, Y. Ma, Z. Zhang, Effect of nano-scale martensite and β phase on the passive film formation and electrochemical behaviour of Ti-¹⁰V-²Fe-3Al alloy in 3.5% NaCl solution, *Electrochim. Acta* 283 (2018) 1300–1312, <https://doi.org/10.1016/j.electacta.2018.07.047>.
- [50] P. Kumar, G.S. Mahobia, S. Mandal, V. Singh, K. Chattopadhyay, Enhanced corrosion resistance of the surface modified Ti-13Nb-13Zr alloy by ultrasonic shot peening, *Corros. Sci.* 189 (2021), 109597, <https://doi.org/10.1016/j.corsci.2021.109597>.
- [51] J.L. Gilbert, P. Khullar, Analysis of electrochemical impedance spectra using phase angle symmetry across log frequency, *J. Electrochem. Soc.* 167 (2020) 21505, <https://iopscience.iop.org/article/10.1149/1945-7111/ab69ff/meta>.
- [52] Y. Zhang, O. Addison, F. Yu, B.C.R. Troconis, J.R. Scully, A.J. Davenport, Time-dependent enhanced corrosion of Ti6Al4V in the presence of H₂O₂ and albumin, *Sci. Rep.* 8 (2018) 3185, <https://doi.org/10.1038/s41598-018-21332-x>.
- [53] E.K. Brooks, R.P. Brooks, M.T. Ehrensberger, Effects of simulated inflammation on the corrosion of 316L stainless steel, *Mater. Sci. Eng. C* 71 (2017) 200–205, <https://doi.org/10.1016/j.msec.2016.10.012>.
- [54] G.J. Brug, A.L.G. van den Eeden, M. Sluyters-Rehbach, J.H. Sluyters, The analysis of electrode impedances complicated by the presence of a constant phase element, *J. Electroanal. Chem. Interfacial Electrochem* 176 (1984) 275–295, [https://doi.org/10.1016/S0022-0728\(84\)80324-1](https://doi.org/10.1016/S0022-0728(84)80324-1).
- [55] M.E. Orazem, B. Tribollet, *Electrochemical Impedance Spectroscopy*, John Wiley & Sons, 2011.
- [56] I. Čaha, A.C. Alves, C. Chirico, A.M. Pinto, S. Tsipas, E. Gordo, O. Bondarchuk, F. L. Deepak, F. Toptan, Atomic-scale investigations of passive film formation on Ti-Nb alloys, *Appl. Surf. Sci.* 615 (2023), 156282, <https://doi.org/10.1016/j.apsusc.2022.156282>.
- [57] S. Pilz, A. Gebert, A. Voss, S. Oswald, M. Göttlicher, U. Hempel, J. Eckert, M. Rohnke, J. Janek, M. Calin, Metal release and cell biological compatibility of beta-type Ti-40Nb containing indium, *J. Biomed. Mater. Res. Part B Appl. Biomater.* 106 (2018) 1686–1697, <https://doi.org/10.1002/jbm.b.33976>.
- [58] N.G. Krishna, R.P. George, J. Philip, Anomalous enhancement of corrosion resistance and antibacterial property of commercially pure Titanium (CP-Ti) with nanoscale rutile titania film, *Corros. Sci.* 172 (2020), 108678, <https://doi.org/10.1016/j.corsci.2020.108678>.
- [59] C.D. Taylor, P. Lu, J. Saal, G.S. Frankel, J.R. Scully, Integrated computational materials engineering of corrosion resistant alloys, *Npj Mater. Degrad.* 2 (2018) 1–10, <https://doi.org/10.1038/s41529-018-0027-4>.
- [60] S. Pilz, A. Hariharan, F. Günther, M. Zimmermann, A. Gebert, Influence of isothermal omega precipitation aging on deformation mechanisms and mechanical properties of a β -type Ti-Nb alloy, *J. Alloy. Compd.* 930 (2023), 167309, <https://doi.org/10.1016/j.jallcom.2022.167309>.
- [61] C. Mao, W. Yu, M. Jin, Y. Wang, X. Shang, L. Lin, X. Zeng, L. Wang, E. Lu, Mechanobiologically optimized Ti-35Nb-2Ta-3Zr improves load transduction and enhances bone remodeling in tilted dental implant therapy, *Bioact. Mater.* 16 (2022) 15–26, <https://doi.org/10.1016/j.bioactmat.2022.03.005>.
- [62] J. Stráský, D. Preisler, H. Seiner, L. Bodnářová, M. Janovská, T. Košťatová, P. Harcuba, K. Salata, K. Halmešová, J. Džugan, Achieving high strength and low elastic modulus in interstitial biomedical Ti-Nb-Zr-O alloys through compositional optimization, *Mater. Sci. Eng. A* 839 (2022), 142833, <https://doi.org/10.1016/j.msea.2022.142833>.
- [63] N.T.C. Oliveira, A.C. Guastaldi, Electrochemical stability and corrosion resistance of Ti-Mo alloys for biomedical applications, *Acta Biomater.* 5 (2009) 399–405, <https://doi.org/10.1016/j.actbio.2008.07.010>.
- [64] D. Mareci, R. Chelariu, D.-M. Gordin, G. Ungureanu, T. Gloriant, Comparative corrosion study of Ti-Ta alloys for dental applications, *Acta Biomater.* 5 (2009) 3625–3639, <https://doi.org/10.1016/j.actbio.2009.05.037>.
- [65] P.F. Ji, B. Li, B.H. Chen, F. Wang, W. Ma, X.Y. Zhang, M.Z. Ma, R.P. Liu, Effect of Nb addition on the stability and biological corrosion resistance of Ti-Zr alloy passivation films, *Corros. Sci.* (2020), 108696, <https://doi.org/10.1016/j.corsci.2020.108696>.
- [66] Y. Gu, A. Ma, J. Jiang, H. Li, D. Song, H. Wu, Y. Yuan, Simultaneously improving mechanical properties and corrosion resistance of pure Ti by continuous ECAP plus short-duration annealing, *Mater. Charact.* 138 (2018) 38–47, <https://doi.org/10.1016/j.matchar.2018.01.050>.
- [67] W.Y. Chen, Y.H. Chen, W.P. Li, R. Zhou, T.H. Chou, X. Wang, J.C. Huang, Passivation evolution of Ti-Ta-Nb medium-entropy sputtered thin films in sulfuric acid solution, *Appl. Surf. Sci.* 576 (2022), 151824, <https://doi.org/10.1016/j.apsusc.2021.151824>.
- [68] Z. Wang, Y. Yan, Y. Wu, X. Huang, Y. Zhang, Y. Su, L. Qiao, Corrosion and tribocorrosion behavior of equiatomic refractory medium entropy TiZr (Hf, Ta, Nb) alloys in chloride solutions, *Corros. Sci.* 199 (2022), 110166, <https://doi.org/10.1016/j.corsci.2022.110166>.
- [69] Y. Bai, Y. Deng, Y. Zheng, Y. Li, R. Zhang, Y. Lv, Q. Zhao, S. Wei, Characterization, corrosion behavior, cellular response and in vivo bone tissue compatibility of titanium-niobium alloy with low Young's modulus, *Mater. Sci. Eng. C* 59 (2016) 565–576, <https://doi.org/10.1016/j.msec.2015.10.062>.

- [70] J. Fojt, L. Joska, J. Malek, V. Sefl, Corrosion behavior of Ti–39Nb alloy for dentistry, *Mater. Sci. Eng. C* 56 (2015) 532–537, <https://doi.org/10.1016/j.msec.2015.07.029>.
- [71] Y. Zhang, A.J. Davenport, B. Burke, N. Vyas, O. Addison, Effect of Zr addition on the corrosion of Ti in acidic and reactive oxygen species (ROS)-containing environments, *ACS Biomater. Sci. Eng.* 4 (2018) 1103–1111, <https://doi.org/10.1021/acsbomaterials.7b00882>.
- [72] C.M. Lousada, M. Jonsson, Kinetics, mechanism, and activation energy of H₂O₂ decomposition on the surface of ZrO₂, *J. Phys. Chem. C* 114 (2010) 11202–11208, <https://doi.org/10.1021/jp1028933>.
- [73] S. Mendis, W. Xu, H.P. Tang, L.A. Jones, D. Liang, R. Thompson, P. Choong, M. Brandt, M. Qian, Characteristics of oxide films on Ti-(10–75) Ta alloys and their corrosion performance in an aerated Hank's balanced salt solution, *Appl. Surf. Sci.* 506 (2020), 145013, <https://doi.org/10.1016/j.apsusc.2019.145013>.